RSC Advances

ROYAL SOCIETY OF CHEMISTRY

www.rsc.org/advances

Revised manuscript submitted to RSC Advances

Date: June 24, 2015

Catalytic Hydrogenation of Isophthalonitrile (IPN) over Supported Monometallic and Bimetallic Catalysts

Chang Liu, Xiaodan Li, Tiefeng Wang*

Beijing Key Laboratory of Green Reaction Engineering and Technology

Department of Chemical Engineering, Tsinghua University, Beijing 100084, China

**Corresponding author: 86-10-62794132, wangtf@tsinghua.edu.cn*

Abstract

The hydrogenation of Isophthalonitrile (IPN) to meta-xylylenediamine (*m*-XDA) is usually catalyzed by the Raney or supported Ni based catalysts in the presence of basic additive. The supported catalysts have better mechanical strength and are safer than Raney Ni catalysts. This work aimed to study the catalytic performance of γ-Al_2O_3 supported Ni and Ni-M (M = Fe, Co, Cu) bimetallic catalysts in IPN hydrogenation. The H_2-TPR results revealed that the introduction of a second metal enhanced the reducibility of Ni catalyst. The Ni-M bimetallic catalysts also had different metal dispersion, electronic property and adsorption strength. Among Fe, Co and Cu, Fe showed the best promoting effect, which was attributed to the strong N-metal bonding and weak H-metal adsorption strength, which enhanced the catalytic activity and *m*-XDA selectivity. The catalytic performance also strongly depended on the Ni-Fe mass ratio. For the γ-Al_2O_3 supported Ni and Ni-M catalysts with a low Ni loading of 5 wt%, the rate constant k_r increased from 0.024 $mol^{0.2}L^{-0.2}min^{-1}$ over $5Ni/Al_2O_3$ to 0.033 $mol^{0.2}L^{-0.2}min^{-1}$ over $5Ni\text{-}1.67Fe/Al_2O_3$, meanwhile the *m*-XDA selectivity increased from 34.7% to 49.5%. Over the Ni-Fe bimetallic catalyst with high metal loading, $20Ni\text{-}5Fe/Al_2O_3$, a very high *m*-XDA selectivity of 99.9% was obtained.

Key words: IPN hydrogenation, supported Ni catalyst, supported bimetallic catalyst

1. Introduction

The hydrogenation of nitriles is an important industrial process to produce primary amines [1-3], which are widely used as solvents, pharmaceuticals, disinfectants, rubber stabilizers, textile additives, and chemical intermediates [4, 5]. The hydrogenation of isophthalonitrile (IPN) to meta-xylylenediamine (*m*-XDA) is usually catalyzed by the Raney or supported Ni based catalysts in the presence of basic additive [3, 5-8]. Raney catalysts have high catalytic activity and selectivity, but low mechanical strength and poor regeneration capability, which causes high catalyst consumption and increases the cost of industrial production [9]. Recently, the supported catalysts with metals from Group VIII as the active component have attracted more attentions [1, 6, 10-15]. The supported catalysts have good mechanical strength provided by the support, and the *m*-XDA selectivity can be enhanced by optimizing the catalyst composition [14, 16-19].

In addition to the hydrogenation reactions, condensation reactions between the highly reactive intermediate imines and amines are the main side reactions in IPN hydrogenation [1, 2, 20, 21]. The condensation reactions decrease the selectivity to *m*-XDA and cause catalyst deactivation by forming higher amines and blocking the catalytic sites. The *m*-XDA selectivity strongly depends on the reaction conditions and catalyst composition. In industrial production, basic additives are usually used to suppress the condensation reactions [5, 11, 15, 22-24]. Our previous studies showed that the acid sites and surface hydroxyl groups on the support could catalyze the condensation reactions [17, 19, 22, 25-27]. By optimizing the preparation method and metal loading, and using K modification, the side reactions had been effectively suppressed over the Ni-Co/γ-Al_2O_3 catalyst [26, 27]. In addition to the reaction conditions and catalyst support, the nature of metal is also crucial for the catalytic activity and product distribution [16]. For nitrile hydrogenation reaction, the metal

components are chosen from group VIII, including precious metals of Pd, Ru, Rh and Pt, and nonprecious metals such as Ni and Co. Among all the active metals investigated, Ni, Co and Ru have the highest selectivity to primary amines, while Rh has a high selectivity to secondary amines, and Pd and Pt have a high selectivity to tertiary amines [15]. Taking into account the catalyst cost, Ni is the most widely used catalyst in the industrial production of *m*-XDA. The catalytic performance of Ni catalysts can be further tuned by adding a second metal, such as Fe, Co, Cu, Pt and Ru.

Bimetallic catalysts have been widely used to promote the catalytic performance of the active metal [28-33]. Yadav et al. [14] studied the SiO_2 supported Ni, Ni-Fe and Ni-Cu catalysts in the liquid-phase hydrogenation of benzonitrile, cinnamonitrile, crotononitrile and butyronitrile. The results showed that the Ni monometallic catalyst and bimetallic catalysts showed the same selectivity but different activity, which was attributed to the structural and electronic effects of the bimetallic alloy. Similar results were also reported by other researchers [6, 29, 31, 33]. A classical theory of ensemble effect and ligand effect was proposed by Sachtler [16] to explain the bimetal interaction. Guczi et al. [33] reported that the three principle effects of adding a second metal were promoter effect by enhancing the reducibility, blocking effect by preventing the migration of the active metal, and synergistic effect by forming bimetallic particles. However, the promotion effect of the second metal has not been fully exploited for IPN hydrogenation reaction, and no commonly accepted conclusions on activity and selectivity have been reported [14, 16].

This work studied the effects of adding a second metal (including Fe, Co, Cu, Pd, and Ru) to the γ-Al_2O_3 supported Ni catalyst on the catalytic performance. The monometallic Ni, Fe, Co, and Cu catalysts were also tested for comparison. The series of monometallic and bimetallic catalysts

were characterized and tested in IPN hydrogenation reaction. The structural and electronic effects of the second metals on the catalytic performance were systematically studied. Among all the added second metals, Fe gave the best promotion effect in enhancing both the catalytic activity and *m*-XDA selectivity.

2. Experimental

2.1. Catalyst preparation

A series of Ni monometallic and bimetallic catalysts were prepared by incipient wetness impregnation using γ-Al_2O_3 as support. The bimetallic catalysts were denoted as *x*Ni-*y*M/Al_2O_3 (M = Fe, Co, Cu), where *x* and *y* are the loadings in wt% of Ni and M, respectively. Nitrates of $Ni(NO_3)_2 \cdot 6H_2O$, $Co(NO_3)_2 \cdot 6H_2O$, $Fe(NO_3)_3 \cdot 9H_2O$ and $Cu(NO_3)_2 \cdot 2.5H_2O$ (98%, Alfa Aesar) were used as metallic precursors and γ-Al_2O_3 (Alfa Aesar, ground to 40–80 mesh) as support. The mass ratio of Ni to M was kept at 4 : 1. Both low (x = 5, y = 1.25) and high (x = 20, y = 5) loadings were studied. Ni and M were impregnated onto the support simultaneously. The impregnated samples were treated with an ultrasonic treatment for 1 h to facilitate metal dispersion, and were aged overnight at room temperature. Then the catalyst samples were dried in air at 80 ^{o}C for 6 h and calcined at 400 ^{o}C for 4 h.

Because the solubility of the nitrates and the water absorption capacity of the supports were low, the catalysts with a high metal loading, namely 20Ni/Al_2O_3 and 20Ni-5M/Al_2O_3, could not be prepared in one impregnation. In this work, repeated impregnation of a calcined catalyst with a lower Ni-M loading was used to prepare the catalysts with high loadings, and 20Ni/Al_2O_3 and 20Ni-5M/Al_2O_3 were prepared by four times of impregnations. The γ-Al_2O_3 supported Ni-Ru and Ni-Pd catalysts were prepared similarly, with the metal loading of 5 wt% Ni and 0.4 wt% Ru or Pd.

The catalysts obtained were stored in vials before use.

2.2. Catalyst characterization

The specific surface area, pore volume and pore size distribution of the unreduced catalysts were determined by N_2 adsorption-desorption with a Quantachrome autosorb iQ and AsiQwin instrument. The results were calculated by the Brunauer-Emmett-Teller (BET) and Barrett-Joyner-Halenda (BJH) methods. Powder X-ray diffraction (XRD) tests of the unreduced catalysts were performed using a Bruker D8 Advance powder X-ray diffractometer (40 kV, 40 mA) with a Cu K_α radiation source and a Ni filter in the 2θ range 5–90°.

The adsorption and reduction properties of the catalysts were measured on a Quantachrome ChemBET Pulsar TPR/TPD instrument. The reducibility of the catalysts was tested by temperature programmed reduction (H_2-TPR) using a 5% H_2/Ar mixture as reducing gas. The consumption of H_2 was measured by a TCD. The CO-uptake of the catalysts was determined by CO chemisorption. Ammonia and hydrogen temperature programmed desorption (NH_3-TPD and H_2-TPD) of the reduced catalysts were also conducted.

The oxidation states of the surface atoms of the unreduced $NiCo/Al_2O_3$ and $3KNiCo/Al_2O_3$ catalysts were examined by XPS (Thermal Scientific ESCALAB 250Xi) with an Al-K_α X-ray source.

2.3. Catalytic reaction

The catalysts were evaluated for the hydrogenation of IPN in a stainless steel autoclave (Weihai Chemical Machinery Co., Ltd., 250 mL). To eliminate the effect of external and internal diffusions so that the catalytic performance can be reliably compared, preliminary experiments were carried out to determine the reaction conditions [34, 35]. Using the catalyst with high activity,

the effects of stirring speed, H_2 flow rate and catalyst particle size were studied. The results showed that the reaction rate increased with increasing stirring speed, and became unchanged at stirring speed above 800 rpm. Similarly, the critical H_2 flow rate and catalyst particle size were also determined. In this study, all the subsequent experiments were carried at stirring speed of 800 rpm, H_2 flow rate of 180 mL min^{-1}, and catalyst particle size of 200–400 μm to ensure that the effect of internal and external diffusions were eliminated., The reaction temperature was 80 ^oC and the pressure was 6.0 MPa. A mixture of 20 mL methanol (> 99.5%, Beijing Chemical Works) and 80 mL toluene (> 99.5%, Beijing Modern Oriental Fine Chemistry Co., Ltd.) was used as the solvent, and 0.086 g NaOH (> 96.0%, Beijing Chemical Works) was used as a basic additive. For each experiment, the amount of IPN (98%, J&K Chemical) was 2.9 g. The amount of catalyst used in each experiment was adjusted to give 0.25 g Ni on the catalyst:

$$\text{Catalyst mass} = \frac{25}{x} \quad (x \text{ in wt\%}) \tag{1}$$

Before each experiment, the catalyst was pre-reduced in H_2 flow of 70 ml min^{-1} at 450 ^oC for 5 h. After passivation in N_2 flow, the reduced catalyst was transferred to the reactant solution in the autoclave. The system was purged with H_2 flow for 30 min under 300 rpm stirring to displace trapped air. Then the reactor system was heated to 80 ^oC under 0.3 MPa and pressurized to 6.0 MPa within 5 min while the H_2 flow rate and stirring speed were set to the specified values. The time when the pressure reached 6.0 MPa was considered as the zero time of the reaction.

The products were sampled online at time intervals of 10 min and were analyzed by a gas chromatograph (GC 7900II, Techcomp Instrument Company) equipped with a DB-1MS UI capillary column (30 m × 0.25 mm × 0.25 μm, Agilent) and an FID detector. The conversion of IPN and the selectivity to *m*-XDA were calculated as:

$$\text{IPN conversion} = \frac{\text{moles of converted IPN}}{\text{moles of IPN feedstock}} \times 100\% \quad (2)$$

$$\text{Product selectivity} = \frac{\text{moles of carbon in a defined product}}{\text{moles of carbon in converted IPN}} \times 100\% \quad (3)$$

The higher amines and other oligomers in the liquid samples could not be detected by GC. To identify the heavier species, some liquid samples were analyzed by mass spectrometry (MS, instrument model: Q Exactive).

3. Results and discussion

3.1. Catalyst Characterization

3.1.1. BET surface area

The physical properties of γ-Al_2O_3 supported Ni monometallic catalysts, Ni based bimetallic catalysts, as well as bare support (calcined before analysis) are listed in Table 1. The support γ-Al_2O_3 had a surface area of 221 $m^2 g^{-1}$ and a pore volume of 0.63 $cm^3 g^{-1}$, which decreased after the introduction of the metal components. For xNi/Al_2O_3, as the Ni loading increased from x = 5 to x = 20, the surface area decreased from 212 to 164 $m^2 g^{-1}$, and the pore volume decreased from 0.59 to 0.44 $cm^3 g^{-1}$, while the average pore diameter remained almost unchanged in the range of 7.84–7.92 nm. Overall, the γ-Al_2O_3 supported xNi-yM bimetallic catalysts had similar specific surface areas, pore volumes and pore sizes to their counterparts of xNi/Al_2O_3. In agreement with the results in the literature [15, 36], the BET results suggested uniform dispersion of Ni or Ni-M on the support, with part of the pore structure blocked by Ni or Ni-M particles at high metal loadings.

3.1.2. XRD

The XRD patterns of the unreduced 20Ni/Al_2O_3, 20Ni-5M/Al_2O_3 and γ-Al_2O_3 are shown in Fig. 1. The XRD patterns of γ-Al_2O_3 showed little change after the introduction of Ni or Ni-M at

the loading of x = 5, which was attributed to the low metal loading and peak overlap of Ni/M oxides and γ-Al_2O_3. At the metal loading of x = 20, the characteristic peaks of NiO were detected.

The introduction of a second metal M (Fe, Co, Cu) changed the XRD patterns of 20Ni/Al_2O_3. The XRD patterns of 20Ni-5Fe/Al_2O_3 and 20Ni-5Cu/Al_2O_3 were similar to that of 20Ni/Al_2O_3, and no characteristic peaks of Fe or Cu were detected due to the high dispersion of Fe and Cu. In addition, the characteristic peaks of NiO were broadened, indicating that the introduction of Fe or Cu increased the NiO dispersion. Different from 20Ni-5Fe/Al_2O_3 and 20Ni-5Cu/Al_2O_3, new characteristic peaks were detected on 20Ni-5Co/Al_2O_3, belonging to Co_3O_4, $NiCo_2O_4$ and Ni/Co aluminates, which were the main phases [37, 38]. The characteristic peaks of NiO were sharpened after the introduction of Co, indicating a lower NiO dispersion on 20Ni-5Co/Al_2O_3 than that on 20Ni/Al_2O_3. To further compare the metal dispersion of the Ni and Ni-M catalysts, the crystal size of NiO on each catalyst was estimated by the Scherrer equation and listed in Table 1. The NiO crystal size was 6.9 nm on 20Ni/Al_2O_3, which decreased to 6.0 nm on 20Ni-5Fe/Al_2O_3 and 5.5 nm on 20Ni-5Cu/Al_2O_3, but increased to 11.4 nm on 20Ni-5Co/Al_2O_3. In addition to the bimetallic promotional effect, the metal loading was also a possible factor for the metal particle size. However, our previous study showed that the metal loading had little effect on the metal particle size for the xNi-yCo/Al_2O_3 catalysts [26, 27]. In this study, we focused on the bimetallic promotional effect, and the effect of the metal loading will be studied in further works.

3.1.3. Catalyst acidity

The acidity of γ-Al_2O_3 support and reduced xNi/Al_2O_3 and xNi-yM/Al_2O_3 catalysts were measured by NH_3-TPD. The total acidity of each sample was calculated from the desorbed amount of NH_3 corresponding to the desorption peak in the range of 100–500 ^oC. The results are

summarized in Table 1. The support γ-Al_2O_3 had some acidity generated from dehydration [39, 40], which was significantly affected by the loading of Ni or Ni-M. The total acidity of γ-Al_2O_3, 5Ni/Al_2O_3 and 20Ni/γ-Al_2O_3 was 0.180, 0.401 and 0.222 mmol NH_3 g^{-1}, respectively. It was reported in the literatures [39, 41, 42] and confirmed in our previous study [27] that the enhanced acidity on the γ-Al_2O_3 supported metal catalysts was attributed to the exposed metal aluminates. The newly formed acid sites only showed acidity when they were exposed and not covered by the loaded metals. Therefore, with increasing metal loading the acidity of the *x*Ni/Al_2O_3 catalysts increased first at low metal loading of $x = 5$ and then decreased at a high metal loading of $x = 20$. The acidity of the Ni-M bimetallic supported catalysts showed similar trend with the metal loading, indicating a similar mechanism of the formation and coverage of the metal aluminates.

3.1.4. H_2-TPR

The H_2-TPR profiles of the *x*Ni-*y*M/Al_2O_3 catalysts are shown in Fig. 2. The results of the corresponding monometallic catalysts Ni/Al_2O_3, Fe/Al_2O_3, Co/Al_2O_3 and Cu/Al_2O_3 with a metal loading of 5.0 wt% are also included for comparison. The monometallic Ni, Fe and Co catalysts are more difficult to reduce than the Cu catalyst, which could result in the significantly different H_2-TPR profiles of Ni-Cu bimetallic catalysts from those of Ni-Fe and Ni-Co.

As shown in Fig. 2(a), the reduction peaks of Ni oxide were at 450 ^oC and in the range of 600–750 ^oC, and those of Fe oxide were at 375 ^oC and 425 ^oC. For all the *x*Ni-*y*Fe/Al_2O_3 catalysts, the reduction of Ni/Fe oxides had two peaks at around 350 ^oC and in the range of 400–750 ^oC, which were lower than that of the characteristic peaks of the monometallic Ni and Fe catalysts. The H_2-TPR results indicated the formation of Ni-Fe bimetallic oxides, which had a higher reducibility than the Ni and Fe monometallic oxides. For example, in the profile of *x*Ni-*y*Fe/Al_2O_3,

the peak at around 350 ^{o}C was due to the reduction of Ni-Fe bimetallic oxides, while the broad peak in the range of 400–750 ^{o}C was due to the reduction of less reducible Ni/Fe monometallic oxides and aluminates. With the increase of Ni-Fe loading, the ratio of Ni/Fe monometallic oxides to Ni-Fe bimetallic oxides increased and the reducibility decreased. In addition, the reduction peak area increased with an increase in the Ni-Fe loading due to the increased amount of the Ni/Fe oxides. As shown in Fig. 2(b), the H_2-TPR patterns of *x*Ni-*y*Co/Al_2O_3 catalysts were similar to those of *x*Ni-*y*Fe/Al_2O_3. The low-loading Ni-Co bimetallic catalysts had two main reduction peaks, namely the peak around 375 ^{o}C belonging to Ni-Co bimetallic oxides, and that in the range of 425–750 ^{o}C belonging to Ni/Co monometallic oxides and Ni/Co aluminates. The first reduction peak slightly splitted into two peaks when the loading increased to x = 20, and the ratio of Ni-Co bimetallic oxides to Ni/Co monometallic oxides decreased. Different from those of *x*Ni-*y*Fe/Al_2O_3 and *x*Ni-*y*Co/Al_2O_3, the H_2-TPR profiles of *x*Ni-*y*Cu/Al_2O_3 were more like the combination of the patterns of Ni and Cu monometallic catalysts. Overall, the introduction of a second metal (Fe, Co and Cu) decreased the reduction temperature and enhanced the reducibility of the Ni supported catalysts.

3.1.5. XPS and CO uptake

The Ni2*p* and Co2*p* binding energies (Ni2$p_{3/2}$ BE and Co2$p_{3/2}$ BE) of the unreduced 5Ni/Al_2O_3, 5Ni-1.25Fe/Al_2O_3, 5Ni-1.25Co/Al_2O_3 and 5Ni-1.25Cu/Al_2O_3 catalysts were analyzed by XPS, and the results were listed in Table 2. The Ni2$p_{3/2}$ BEs were around 855 eV, which belonged to the Ni(II) oxidation state [43]. The introduction of a second metal had important effects on the surface properties [6]. The Ni2$p_{3/2}$ BE decreased from 855.57 eV on 5Ni/Al_2O_3 to 855.03 eV on 5Ni-1.25Fe/Al_2O_3 and 855.12 eV on 5Ni-1.25Cu/Al_2O_3, but increased to 855.78 eV on

5Ni-1.25Co/Al_2O_3. The Ni2$p_{3/2}$ BE was an index of electron density, and the lower Ni2$p_{3/2}$ BE on Ni-Fe and Ni-Cu bimetallic catalysts indicated a higher electron density of Ni surface atoms than on the Ni monometallic catalyst. The introduction of Fe, Co or Cu also affected the surface concentration of Ni and Ni + M. As shown in Table 2, the Ni/Al surface atomic ratio decreased from 0.099 on 5Ni/Al_2O_3 to 0.088–0.096 on the Ni-M bimetallic catalysts, with the lowest value on Ni-Co. The (Ni+M)/Al surface atomic ratio increased from 0.099 on 5Ni/Al_2O_3 to 0.100–0.146 on the bimetallic catalysts, and the significantly higher ratio on Ni-Fe bimetal was due to the enrichment of Fe on the catalyst surface [31].

The reduced 5Ni/Al_2O_3 and 5Ni-1.25M/Al_2O_3 catalysts were characterized by CO chemisorption. The CO-uptake of 5Ni/Al_2O_3, 5Ni-1.25Fe/Al_2O_3, 5Ni-1.25Co/Al_2O_3 and 5Ni-1.25Cu/Al_2O_3 were 24.8, 32.2, 14.4 and 57.5 μmol g^{-1}, respectively. Assuming a chemisorption stoichiometric factor of 1.0 for Ni, Fe, Co, and Cu, the metal dispersion was 2.80% on Ni-Fe, 1.35% on Ni-Co, and 5.49% on Ni-Cu. Among Fe, Co and Cu, the addition of Cu to Ni significantly enhanced the metal dispersion, while Co decreased the metal dispersion.

3.1.6. H_2-TPD

The reduced 5Ni/Al_2O_3 and 5Ni-1.25M/Al_2O_3 catalysts were characterized by H_2-TPD, as shown in Fig. 3. The monometallic 5Ni/Al_2O_3 had two main desorption peaks at 460 ^oC and 550 ^oC. The H_2-TPD profiles of the bimetallic catalyst 5Ni-1.25M/Al_2O_3 were very different from that of 5Ni/Al_2O_3. The Ni-Fe and Ni-Co bimetallic catalysts had two main H_2 desorption peaks. For 5Ni-1.25Fe/Al_2O_3, the first peak shifted to a lower temperature (400 ^oC), along with an increase in the peak area. For 5Ni-1.25Co/Al_2O_3, the second peak shifted to a higher temperature (580 ^oC), and the peak area significantly deceased compared with that of 5Ni/Al_2O_3. The 5Ni-1.25Cu/Al_2O_3

catalyst had three main H_2 desorption peaks, with one additional peak to those of the two main peaks of 5Ni/Al_2O_3. The first peak of 5Ni-1.25Cu/Al_2O_3 was at about 400 ^oC, which was close to the first peak of 5Ni-1.25Fe/Al_2O_3. According to the literatures [38, 44, 45], the peaks at low temperatures were generally attributed to the chemisorbed hydrogen on the metal particles, while those at high temperatures were ascribed to the spillover hydrogen on the support. As reported in the literatures [6, 29, 38], the desorption temperature was an index of the H-metal interaction, and the peak area was that of metal exposure and adsorption capacity. The H_2-TPD results indicated that the introduction of Fe increased the metal exposure and decreased the H adsorption, the introduction of Cu enhanced both the metal exposure and adsorption strength, whereas the introduction of Co decreased the exposure and maintained the adsorption strength.

3.2. Catalytic performance

3.2.1. Bimetallic synergy effect

The *x*Ni/Al_2O_3 and *x*Ni-*y*M/Al_2O_3 catalysts were evaluated in the IPN hydrogenation reaction under the same conditions in the presence of 0.086 g NaOH as basic additive. The conversion of IPN and selectivity to *m*-XDA are plotted as a function of the reaction time in Fig. 4. The rate constant (k_r) and *m*-XDA selectivity over *x*Ni/Al_2O_3 and *x*Ni-*y*M/Al_2O_3 are listed in Table 3. The reaction order (p) and rate constant (k_r) were determined by fitting the IPN concentration data in the first 100 min as a function of the reaction time using Eq. (4).

$$\frac{\mathrm{d}C_{\mathrm{IPN}}}{\mathrm{d}t} = -k_{\mathrm{r}} C_{\mathrm{IPN}}^{p} \quad (4)$$

The regression results showed that the apparent reaction order of 0.8 fitted all the experimental data well. At the Ni loading of 5 wt%, the rate constant k_r was 0.024, 0.025, 0.029

and 0.021 $mol^{0.2}$ $L^{-0.2}$ min^{-1}, respectively, over $5Ni/Al_2O_3$, $5Ni\text{-}1.25Cu/Al_2O_3$, $5Ni\text{-}1.25Fe/Al_2O_3$ and $5Ni\text{-}1.25Co/Al_2O_3$. The metal component also affected the selectivity to *m*-XDA. The selectivity to *m*-XDA was 34.7% over $5Ni/Al_2O_3$, which was almost unchanged after the introduction of Cu, but increased to 45.5% over $5Ni\text{-}1.25Co/Al_2O_3$ and to 47.4% over $5Ni\text{-}1.25Fe/Al_2O_3$. In our previous work [26], mass spectra measurements showed that the enhanced formation of higher amines was responsible for the low selectivity to *m*-XDA. At Ni loading of 20 wt%, the reaction rate constant k_r and *m*-XDA selectivity were higher than those over the $5Ni(\text{-}1.25M)/Al_2O_3$ catalysts. Similar to the results over $5Ni/Al_2O_3$ and $5Ni\text{-}1.25M/Al_2O_3$, the rate constant showed similar trend with the metal composition, which increased from 0.031 $mol^{0.2}$ $L^{-0.2}$ min^{-1} over $20Ni/Al_2O_3$ to 0.041 and 0.042 $mol^{0.2}$ $L^{-0.2}$ min^{-1} over $20Ni\text{-}5Fe/Al_2O_3$ and $20Ni\text{-}5Cu/Al_2O_3$, respectively, but decreased to 0.028 $mol^{0.2}$ $L^{-0.2}$ min^{-1} over $20Ni\text{-}5Co/Al_2O_3$. Compared with the results over the $5Ni/Al_2O_3$ and $5Ni\text{-}1.25M/Al_2O_3$ catalysts, the *m*-XDA selectivity over the bimetallic catalysts of 20 wt% Ni was much higher (99.9% over $20Ni\text{-}5Fe/Al_2O_3$, 99.9% over $20Ni\text{-}5Co/Al_2O_3$, and 96.8% over $20Ni\text{-}5Cu/Al_2O_3$), and also showed bimetallic promoting effect (93.9% *m*-XDA selectivity over $20Ni/Al_2O_3$).

The $5Ni\text{-}0.4Pd/Al_2O_3$ and $5Ni\text{-}0.4Ru/Al_2O_3$ catalysts were also evaluated in the IPN hydrogenation reaction for comparison. The results showed that the Ni-Pd and Ni-Ru bimetallic catalysts had much higher catalytic activity than the Ni monometallic and Ni-M (M = Fe, Co, Cu) bimetallic catalysts, but had much lower *m*-XDA selectivity, which was only 11.1% over $5Ni\text{-}0.4Pd/Al_2O_3$ and 29.3% over $5Ni\text{-}0.4Ru/Al_2O_3$. These results were consistent with the literature [16]. Overall, the catalytic results of $x Ni/Al_2O_3$ and $x Ni\text{-}y M/Al_2O_3$ showed that the introduction of a second metal had significant effects on the activity and selectivity. The addition

of Cu to the Ni based catalyst mainly enhanced the catalytic activity, and the addition of Co increased the *m*-XDA selectivity but decreased the activity. Fe showed the best promoting effects both in catalytic activity and *m*-XDA selectivity.

3.2.2. Effect of structural and electronic properties

By correlating the catalyst characterization and reaction results, the trend in the activity and *m*-XDA selectivity could be well explained. The characterization results of BET, XRD and NH_3-TPD showed that the morphology, metal-support interaction and the main metal speciation of the monometallic and bimetallic catalysts were almost independent of the metal composition. However, the XRD, CO uptake and H_2-TPD results show that the metal dispersion was affected by the metal composition. The introduction of Fe and Cu as the second metal increased the metal dispersion, while that of Co decreased the metal dispersion. It has been reported that the catalyst for nitrile hydrogenation is structure sensitive, but there still existed controversy about the effect of the metal size on catalytic activity [18, 46, 47]. The studies of Arai et al. [46] and Rode et al. [18] showed that with decreasing degree of metal dispersion, the turnover frequency (TOF) of nitrile hydrogenation reaction increased, while Bond et al. [47] indicated the opposite trend. In this study, the results showed that the catalytic activity increased with increasing metal dispersion.

The adsorption property of the Ni catalyst was changed by the introduction of a second metal. According to the XPS results, the electron density of Ni increased on Ni-Fe and Ni-Cu, and decreased on Ni-Co. The study of Yadav et al. [14] showed that the electron-rich Ni sites favored the adsorption of nitriles by enhancing the N-metal bonding, and therefore weakened the strength of C≡N or C=N and facilitated the attack of adsorbed H atom to the C≡N or C=N groups in the IPN hydrogenation. The H_2-TPD results indicated that the H adsorption capacity was enhanced on

Ni-Fe and Ni-Cu, and reduced on Ni-Co bimetallic catalysts, compared with the Ni monometallic catalyst [38].

In this study, the difference in activity and *m*-XDA selectivity on Ni and Ni-M catalysts was attributed to the combination of the structural and electronic properties. Strong N-metal interaction and weak H-metal adsorption favored the selective hydrogenation of IPN to *m*-XDA. Take the $5Ni/Al_2O_3$ and $5Ni\text{-}1.25M/Al_2O_3$ catalysts for example, compared with the Ni monometallic catalyst, the Ni-Fe bimetallic catalyst had a higher metal dispersion and more active sites. The bonding of C≡N and C=N groups were enhanced due to the enriched electron density on Ni. Besides, the Ni-Fe bimetallic catalysts could adsorb more H at weaker strength. Overall, the high metal dispersion, strong N-metal bonding and weak H-metal adsorption strength of the Ni-Fe bimetallic catalysts increased the catalytic activity, and prevented the desorption of imines from the metal sites and occurrence of subsequent condensation reactions, thus increased the selectivity to *m*-XDA. Compared with Ni-Fe, the Ni-Cu bimetallic catalysts had a weaker N-metal interaction and a stronger H-metal adsorption strength, therefore the H atoms were difficult to desorb from the metal sites to attack the C≡N and C=N groups for hydrogenation reaction. Besides, the formed imines were easier to desorb from the metal sites to produce higher amines. Among all the bimetallic catalysts, the Ni-Co bimetallic catalysts had the lowest metal dispersion and H adsorption capacity, leading to a low hydrogenation activity. The *m*-XDA selectivity over the Ni-Co bimetallic catalysts was higher than that over the Ni monometallic catalysts, which could be attributed to the effect of the nature of metal component.

For the catalysts with a high metal loading (x = 20), the difference between the bimetallic catalysts was similar to that of the low-loading bimetallic catalysts, but in a smaller extend, due to

the decreased amount of "adverse" sites, namely the acid sites and surface hydroxyl groups [27], on which the condensation side reactions occurred.

3.2.3. Effect of composition on Ni-Fe bimetallic catalysts

To study the effect of the composition on catalytic performance, and get the best activity and *m*-XDA selectivity, the Ni-Fe ratio was optimized for the Ni-Fe bimetallic catalysts. For a better comparison, the catalysts with lower metal loading that had lower *m*-XDA selectivity were evaluated. The results were shown in Fig. 5.

The effect of the Ni/Fe mass ratio was studied by changing the Ni/Fe mass ratio while keeping the total loading of Ni and Fe at 6.25 wt%. As shown in Fig. 5(a), Fe alone showed almost no activity for the IPN hydrogenation reaction. Additional experiments showed Co and Cu monometallic catalysts were also inactive for the IPN hydrogenation reaction. By adding a moderate mass ratio of Fe (Fe/(Ni+Fe) = 0.2 or 0.6) to the Ni monometallic catalyst, both the activity and selectivity were enhanced, and the best catalytic performance was obtained at Fe/(Ni+Fe) = 0.2. Considering that Fe had a very low catalytic activity for IPN hydrogenation, the catalyst composition was further optimized based on the 5 wt%Ni catalyst, as shown in Fig. 5(b). The optimal Ni-Fe mass ratio was 1.67Fe/5Ni, at which the rate constant increased to 3.3×10^{-2} $mol^{0.2}$ $L^{-0.2}$ min^{-1} from 2.9×10^{-2} $mol^{0.2}$ $L^{-0.2}$ min^{-1} over 5Ni-1.25Fe/Al_2O_3 and the *m*-XDA selectivity increased to 49.5% from 47.4% over 5Ni-1.25Fe/Al_2O_3.

4. Conclusions

The *x*Ni/Al_2O_3 and *x*Ni-*y*M/Al_2O_3 (M = Fe, Co, Cu, Pd and Ru) monometallic and bimetallic catalysts were prepared and evaluated for the IPN hydrogenation reaction. Catalyst characterization showed that the physical morphology, metal-support interaction and the main

metal speciation were almost unchanged by the introduction of the second metal. Compared with the Ni monometallic catalysts, the bimetallic catalysts had better reducibility. The metal dispersion, electronic property and adsorption strength were also affected by the bimetallic interaction between Ni and the added metal Fe, Co and Cu. Among the Ni, Fe, Co and Cu monometallic catalysts and Ni-M (M = Fe, Co, Cu) bimetallic catalysts, the Ni-Fe bimetallic catalysts had strong N-metal bonding, weak H-metal adsorption strength and large H adsorption capacity, thus increased both the catalytic activity and *m*-XDA selectivity. The Ni-Fe catalyst was further optimized by changing the Ni/Fe mass ratio. For the γ-Al_2O_3 supported Ni and Ni-M catalysts with a low Ni loading of 5 wt%, the rate constant k_r increased from 0.024 $mol^{0.2}L^{-0.2}min^{-1}$ over $5Ni/Al_2O_3$ to 0.033 $mol^{0.2}L^{-0.2}min^{-1}$ over $5Ni\text{-}1.67Fe/Al_2O_3$, meanwhile the *m*-XDA selectivity increased from 34.7% to 49.5%. Over the Ni-Fe bimetallic catalysts with high metal loading ($20Ni\text{-}5Fe/Al_2O_3$), a high *m*-XDA selectivity of 99.9% was obtained.

Acknowledgement

This work was supported by Program for New Century Excellent Talents in University of China (NCET-12-0297).

References

1 Y. Huang, W. M. H. Sachtler, *Appl. Catal., A.*, 1999, **182**, 365-378.

2 C. De Bellefon, P. Fouilloux, *Catal. Rev.*, 1994, **36**, 459-506.

3 B.W. Hoffer, J.A. Moulijn, *Appl. Catal., A.*, 2009, **352**, 193-201.

4 R. K. Marella, K. S. Koppadi, Y.Jyothi, K. S. R. Rao, D. R. Burri, *New J. Chem.*, 2013, **37**, 3229.

5 S. W. Row, T. Y. Chae, K. S. Yoo, S. D. Lee, D. W. Lee, Y. Shul, *Can. J. Chem. Eng.*, 2007, **85**, 925-928.

6 T. Shi, H. Li, L.Yao, W. Ji, C. T. Au, *Appl. Catal., A.*, 2012, **425**, 68-73.

7 T. Y. Chae, S. W. Row, K. S. Yoo, S. D. Lee, D. W. Lee, *Bull. Korean Chem. Soc.*, 2006, **27**, 361-362.

8 F. Hochard, H. Jobic, J. Massardier, A. J. Renouprez, *J. Mol. Catal. A-Chem.*, 1995, **95**, 165-172.

9 B. W. Hoffer, *Tuning Raney-type and Supported Ni Catalysts for Commercial Hydrogenation Reactions*, 2003.

10 L. Hegedűs, T. Máthé, T. Kárpáti, *Appl. Catal., A.*, 2008, **349**, 40-45.

11 Y. Huang, *J. Catal.*, 2000, **190**, 69-74.

12 M.H.G. Prechtl, J.D. Scholten, J. Dupont, *J. Mol. Catal. A-Chem.*, 2009, **313**, 74-78.

13 P. Braos-García, C. García-Sancho, A. Infantes-Molina, E. Rodríguez-Castellón, A. Jiménez-López, *Appl. Catal., A.*, 2010, **381**, 132-144.

14 G. D. Yadav, M.R. Kharkara, *Appl. Catal., A.*, 1995, **126**, 115-123.

15 D. J. Segobia, A. F. Trasarti, C.R. Apesteguía, *Appl. Catal., A.*, 2012, **445**, 69-75.

16 Y. Huang, M.M.H. Sachtler, *J. Catal.*, 1999, **188**, 215-225.

17 M. J. F. M. Verhaak, *Catal. Lett.*, 1994, **26**, 37-53.

18 C. V. Rode, M. Arai, M. Shirai, Y. Nishiyama, *Appl. Catal., A.*, 1997, **148**, 405-413.

19 A. Infantesmolina, *J. Catal.*, 2004, **225**, 479-488.

20 P. Scharringer, T. Muller, J. Lercher, *J. Catal.*, 2008, **253**, 167-179.

21 J. V. Braun, G. Blessing, F. Zobel, *Berichte der deutschen chemischen Gesellschaft (A and B Series)*, 1923, **56**, 1988-2001.

22 F. M. Cabello, D. Tichit, B. Coq, A. Vaccari, N. T. Dung, *J. Catal.*, 1997, **167**, 142-152.

23 W. H. Hartung, *J. Am. Chem. Soc.*, 1928, **50**, 3370-3374.

24 S. Gomez, J. A. Peters, T. Maschmeyer, *Adv. Synth. Catal.*, 2002, **344**, 1037-1057.

25 H. Chen, M. Xue, S. Hu, *J. Shen, Chem. Eng. J.*, 2012, **181**, 677-684.

26 C. Liu, T. Wang, *Rsc Adv.*, 2014, **109**, 63725-63733.

27 C. Liu C, R. Hou, T. Wang, *Rsc Adv.*, 2015, **5**, 26465-26474.

28 H. Kusaka, Y. Hara, M. Onuki, T. Akai, M. Okuda, *J. Catal.*, 1996, **161**, 96-106.

29 M. Arai, T. Ebina, M. Shirai, *Appl. Surf. Sci.*, 1999, **148**, 155-163.

30 R. M. Deshpande, V. V. Buwa, C. V. Rode, R. V. Chaudhari, P. L. Mills, *Catal. Commun.*, 2002, **3**, 269-274.

31 T. Ishiharaa, K. E. H. Araia, *Appl. Catal.*, 1987, **30**, 225-238.

32 G. K. Reddy, K. N. Rao, A. Khan, I. Ganesh, *J. Mol. Catal. A-Chem.*, 2007, **265**, 276-282.

33 L. Guczi, I. Kiricsi, *Appl. Catal., A.*, 1999, **186**, 375-394.

34 Z. Zhao, Y. Fang, P. J. J Alvarez, M. S. Wong, *Appl. Catal., B.*, 2013, **140-141**, 468-477.

35 Z. Zhao, J. Arentz, L. A. Pretzer, P. Limpornpipat, J. M. Clomburg, R. Gonzalez, N. M. Schweitzer, T. Wu, J. T. Miller, M. S. Wong, *Chem . Sci.*, 2014, **5**, 3715-3728.

36 A. Gluhoi, N. Bogdanchikova, B. Nieuwenhuys, *J. Catal.*, 2005, **232**, 96-101.

37 A. A. Khassin, T. M. Yurieva, V. V. Kaichev, V. I. Bukhtiyarov, A. A. Budneva, E. A. Paukshtis, *J. Mol. Catal. A-Chem.*, 2001, **175**, 189-204.

38 D. Xu, W. Li, H. Duan, Q. Ge, H. Xu, *Catal. Lett.*, 2005, **102**, 229-235.

39 P. De Bokx, W. Wassenberg, J. Geus, *J. Catal.*, 1987, **104**, 86-98.

40 H. H. Lu, Y. M. Liu, Q. I. Lin, H. B. Yin, *Mod. Chem. Ind.*, 2008, **28**, 55-57.

41 W. D. Mross, *Cat. Rev.*, 1983, **25**, 591-637.

42 S. Benbenek, E. Fedoryńska, P. Winiarek, *React. Kinet. Catal. Lett.*, 1993, **51**, 189-195.

43 A. P. Grosvenor, M. C. Biesinger, R. S. C. Smart, N. S. Mcintyre, *Surf. Sci.*, 2006, **600**, 1771-1779.

44 S. Velu, S. Gangwal, *Solid State Ion.*, 2006, **177**, 803-811.

45 A. G. Boudjahem, S. Monteverdi, M. Mercy, D. Ghanbaja, M. M. Bettahar, *Catal. Lett.*, 2002, **84**, 115-122.

46 M. Arai, Y. Takada, Y. Nishiyama, *J. Phys. Chem. B*, 1998, **102**, 1968-1973.

47 G. Bond, F.S. Stone, *Stud. Surf. Sci. Catal.*, 1996, **96**, 257–266.

Table captions

Table 1. Physical properties, acidity and NiO crystal size of *x*Ni/Al_2O_3, *x*Ni-*y*M/Al_2O_3 and γ-Al_2O_3

Table 2. XPS and CO uptake results of 5Ni/Al_2O_3 and 5Ni-1.25M/Al_2O_3

Table 3. Reaction results of *x*Ni/Al_2O_3 and *x*Ni-*y*M/Al_2O_3 catalysts

Table 1. Physical properties, acidity and NiO crystal size of xNi/Al_2O_3, xNi-yM/Al_2O_3 and γ-Al_2O_3

Catalyst	S (m^2 g^{-1}) [a]	V_p (cm^3 g^{-1}) [a]	D_p (nm) [a]	Acidity (mmol NH_3 g^{-1}) [a]	Crystal size of NiO (nm) [b]
γ-Al_2O_3	221	0.63	7.92	0.180	/
Ni	212 (164)	0.59 (0.44)	7.92 (7.84)	0.401 (0.222)	6.9
Ni-Fe	209 (152)	0.57 (0.35)	7.87 (7.88)	0.513 (0.203)	6.0
Ni-Co	209 (153)	0.57 (0.41)	7.89 (7.90)	0.474 (0.160)	11.4
Ni-Cu	205 (149)	0.57 (0.38)	7.90 (7.86)	0.374 (0.186)	5.5

[a] The numbers in brackets are results of 20Ni(-5M)/Al_2O_3, and those outside the brackets are results of 5Ni(-1.25M)/Al_2O_3, M = Fe, Co, Cu.

[b] The results of NiO crystal size were those of 20Ni(-5M)/Al_2O_3, calculated from the characteristic peak at 43 °.

Table 2. XPS and CO uptake results of $5Ni/Al_2O_3$ and $5Ni\text{-}1.25M/Al_2O_3$

	$5Ni/Al_2O_3$	$5Ni\text{-}1.25Fe/Al_2O_3$	$5Ni\text{-}1.25Co/Al_2O_3$	$5Ni\text{-}1.25Cu/Al_2O_3$
Ni2$p_{3/2}$ BE (eV)	855.57	855.03	855.78	855.12
Ni/Al ratio	0.099	0.091	0.088	0.096
(Ni+M)/Al ratio	0.099	0.146	0.100	0.109
CO uptake (μmol g^{-1})	24.8	32.2	14.4	57.5
Metal dispersion (%) [a]	2.91	2.80	1.35	5.49

[a] Metal dispersion was calculated by assuming a chemisorption stoichiometric factor of 1.0 for Ni, Fe, Co and Cu.

Table 3. Reaction results of xNi/Al_2O_3 and xNi-yM/Al_2O_3 catalysts

Catalyst	Reaction results[a]	
	k_r(10^{-2} $mol^{0.2}$ $L^{-0.2}$ min^{-1})	Selectivity to *m*-XDA (%)
Ni[b]	2.4 (3.1)	34.7 (93.9)
Ni-Fe[b]	2.9 (4.1)	47.4 (99.9)
Ni-Co[b]	2.1 (2.8)	45.5 (99.9)
Ni-Cu[b]	2.5 (4.2)	34.7 (96.8)

[a] Reaction conditions: 80 °C, 6.0 MPa, catalyst in 200~400 μm containing 0.25 g Ni, 80 mL of toluene and 20 mL of methanol as solvent, 2.9 g of IPN feed, 0.086g NaOH as basic additives, 180 mL min^{-1} H_2 gas flow, and stirring speed of 800 rpm.

[b] The numbers in brackets are results of 20Ni(-5M)/Al_2O_3, and those outside the brackets are results of 5Ni(-1.25M)/Al_2O_3, M = Fe, Co, Cu.

Figure captions

Fig. 1. XRD profile of 20Ni/Al_2O_3, 20Ni-5M/Al_2O_3 and γ-Al_2O_3

Fig. 2. H_2-TPR results of γ-Al_2O_3 supported monometallic and bimetallic catalysts (a) Ni, Fe and Ni-Fe; (b) Ni, Co and Ni-Co; and (c) Ni, Cu and Ni-Cu

Fig. 3. H_2-TPD results of 5Ni/Al_2O_3 and 5Ni-1.25M/Al_2O_3

Fig. 4. Catalytic performance of *x*Ni/Al_2O_3 and *x*Ni-*y*M/Al_2O_3

(a) IPN conversion, (b) *m*-XDA selectivity over 5Ni/Al_2O_3 and 5Ni-1.25M/Al_2O_3;

(c) IPN conversion, (d) *m*-XDA selectivity over 20Ni/Al_2O_3 and 20Ni-5M/Al_2O_3

Fig. 5. Effect of the Ni-Fe ratio on catalytic performance of Ni-Fe/Al_2O_3 catalysts (a) Ni + Fe = 6.25 wt%, (b) Ni = 5 wt%

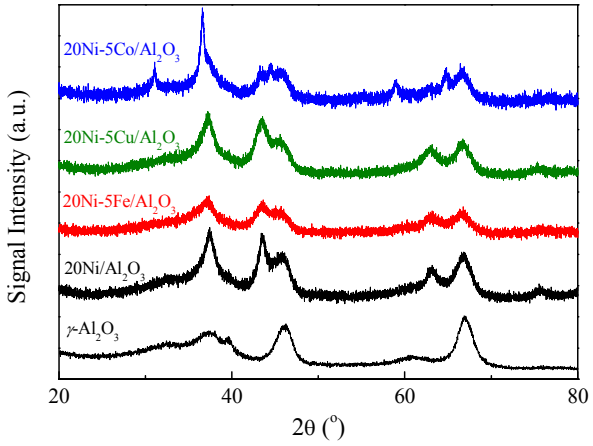

Fig. 1. XRD profile of $20Ni/Al_2O_3$, $20Ni\text{-}5M/Al_2O_3$ and $\gamma\text{-}Al_2O_3$

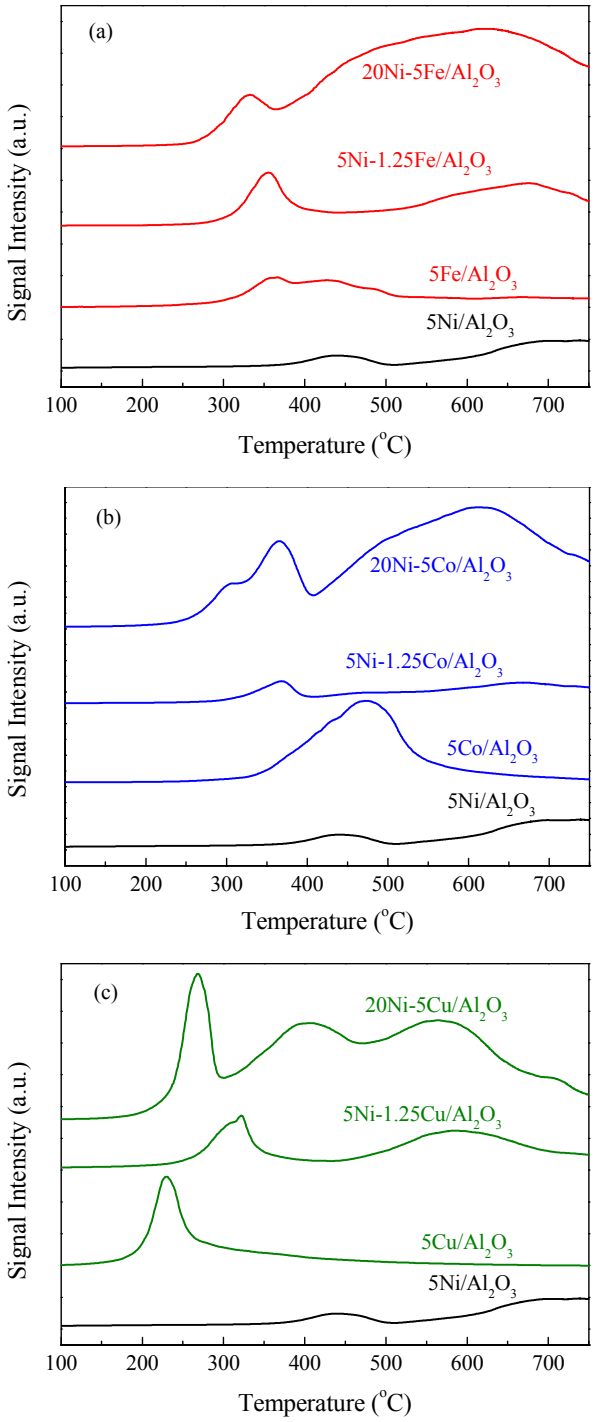

Fig. 2. H_2-TPR results of γ-Al_2O_3 supported monometallic and bimetallic catalysts (a) Ni, Fe and Ni-Fe; (b) Ni, Co and Ni-Co; and (c) Ni, Cu and Ni-Cu

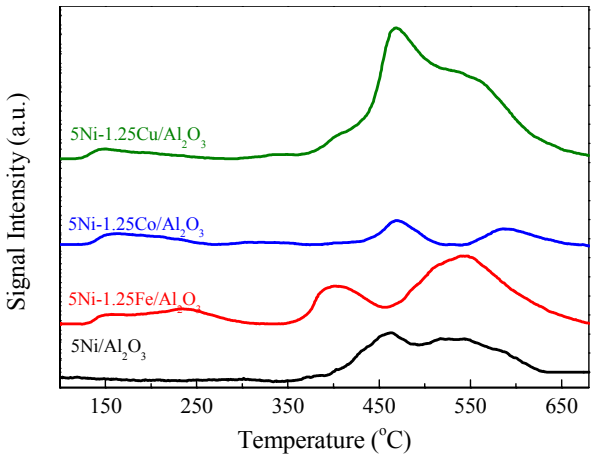

Fig. 3. H_2-TPD results of $5Ni/Al_2O_3$ and $5Ni\text{-}1.25M/Al_2O_3$

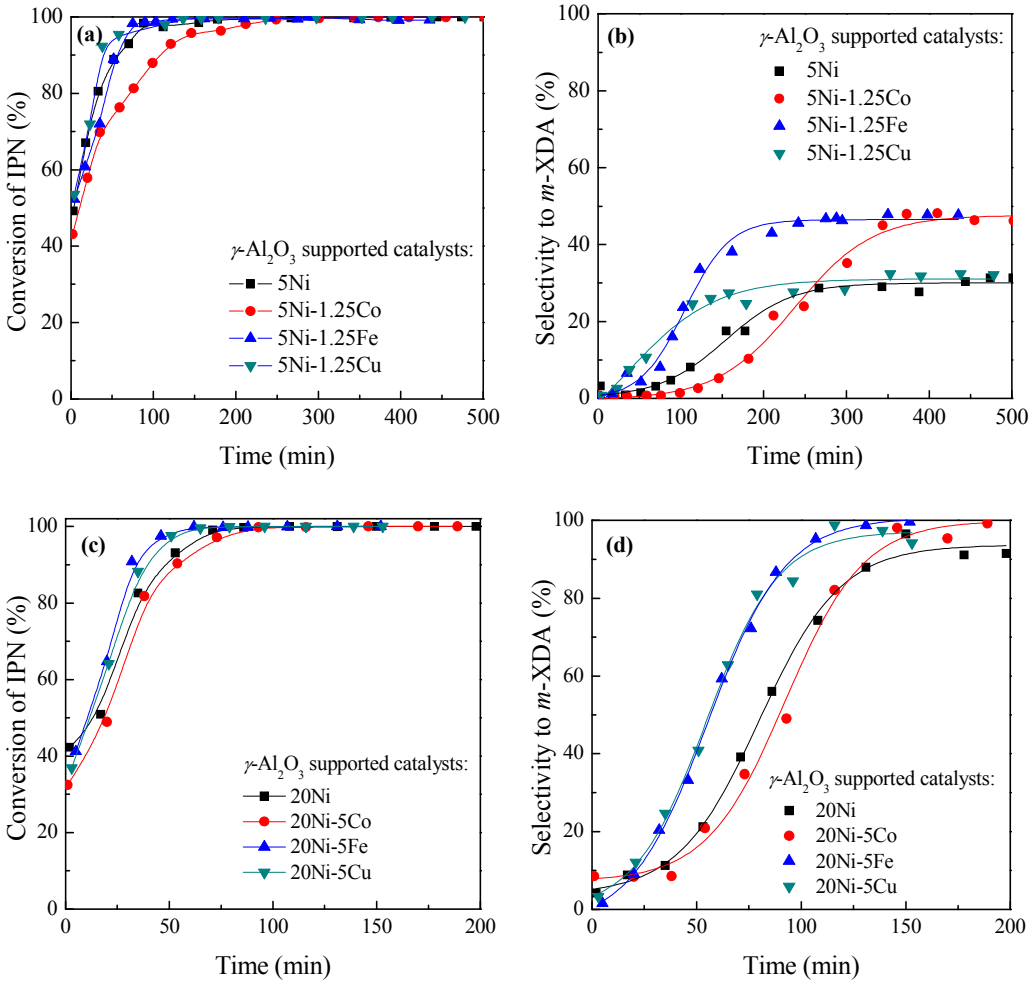

Fig. 4. Catalytic performance of xNi/Al_2O_3 and xNi-yM/Al_2O_3

(a) IPN conversion, (b) *m*-XDA selectivity over 5Ni/Al_2O_3 and 5Ni-1.25M/Al_2O_3;

(c) IPN conversion, (d) *m*-XDA selectivity over 20Ni/Al_2O_3 and 20Ni-5M/Al_2O_3

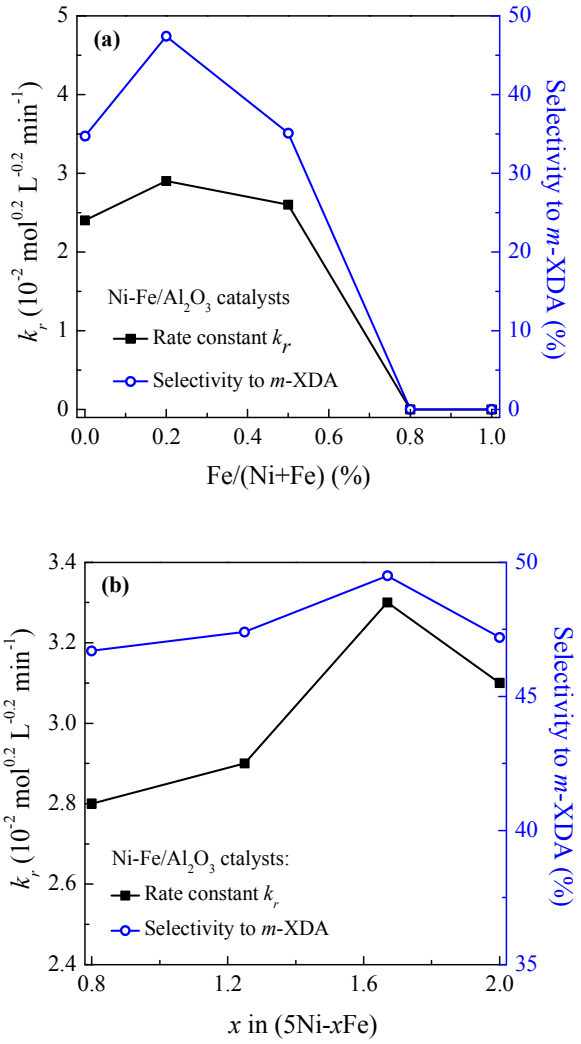

Fig. 5. Effect of the Ni-Fe ratio on catalytic performance of Ni-Fe/Al_2O_3 catalysts (a) Ni + Fe = 6.25 wt%, (b) Ni = 5 wt%

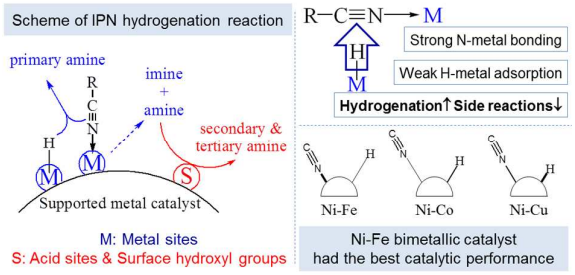

The Ni-Fe/γ-Al_2O_3 bimetallic catalyst showed enhanced activity and *m*-XDA selectivity in hydrogenation of IPN, due to strong N-metal interaction and weak H adsorption strength.